

Encapsulation of Non-Precious Metal into Ordered Mesoporous N-Doped Carbon for Efficient Quinoline Transfer Hydrogenation with Formic Acid

Guoqiang Li, Huanhuan Yang, Haifu Zhang, Zhiyuan Qi, Minda Chen, Wei Hu, Lihong Tian, Renfeng Nie, and Wenyu Huang

ACS Catal., **Just Accepted Manuscript** • DOI: 10.1021/acscatal.8b01404 • Publication Date (Web): 27 Jul 2018

Downloaded from <http://pubs.acs.org> on July 27, 2018

Just Accepted

“Just Accepted” manuscripts have been peer-reviewed and accepted for publication. They are posted online prior to technical editing, formatting for publication and author proofing. The American Chemical Society provides “Just Accepted” as a service to the research community to expedite the dissemination of scientific material as soon as possible after acceptance. “Just Accepted” manuscripts appear in full in PDF format accompanied by an HTML abstract. “Just Accepted” manuscripts have been fully peer reviewed, but should not be considered the official version of record. They are citable by the Digital Object Identifier (DOI®). “Just Accepted” is an optional service offered to authors. Therefore, the “Just Accepted” Web site may not include all articles that will be published in the journal. After a manuscript is technically edited and formatted, it will be removed from the “Just Accepted” Web site and published as an ASAP article. Note that technical editing may introduce minor changes to the manuscript text and/or graphics which could affect content, and all legal disclaimers and ethical guidelines that apply to the journal pertain. ACS cannot be held responsible for errors or consequences arising from the use of information contained in these “Just Accepted” manuscripts.



1
2
3
4
5
6
7 Encapsulation of Non-Precious Metal into Ordered
8
9
10 Mesoporous N-Doped Carbon for Efficient
11
12
13
14
15 Quinoline Transfer Hydrogenation with Formic Acid
16
17
18
19

20 *Guoqiang Li,¹ Huanhuan Yang,¹ Haifu Zhang,¹ Zhiyuan Qi,² Minda Chen,² Wei Hu,¹ Lihong*
21 *Tian,¹ Renfeng Nie,^{*1,2} Wenyu Huang^{*2}*
22
23
24
25
26

27 ¹ Hubei Collaborative Innovation Center for Advanced Organic Chemical Materials, & Ministry-
28 of-Education Key Laboratory for the Synthesis and Application of Organic Functional
29 Molecules, School of Chemistry and Chemical Engineering, Hubei University, Wuhan 430062,
30
31
32
33
34 P.R. China
35

36 ² Department of Chemistry, Iowa State University, Ames, Iowa 50011, USA
37
38
39
40

41 ABSTRACT: Ordered mesoporous N-doped carbon (OMNC) encapsulating Co nanoparticles
42 (NPs) have been prepared under direct polymerization between $[\text{Co}(\text{NH}_2\text{CH}_2\text{CH}_2\text{NH}_2)_2]\text{Cl}_2$ and
43 carbon tetrachloride through a hard template method. The catalysts (Co@OMNC) are pyrolyzed
44
45
46
47
48
49
50
51
52
53
54
55
56
57
58
59
60
the quinoline transfer hydrogenation with formic acid (FA) as the hydrogen source under a base-free condition, the encapsulated Co NPs are physically isolated from the acidic reaction solution, which prevents them from poisoning or leaching. The rich mesopores and N dopants afford

1
2
3 enhanced adsorption of quinoline. Co@OMNC-700 (pyrolyzed at 700 °C) gives best activity
4 (98.8 % conversion) as well as 100 % 1,2,3,4-tetrahydroquinoline (THQ) selectivity at 140 °C
5
6 for 4h, exhibiting significantly improved performance than using H₂ as the hydrogenation source.
7
8 Moreover, Co@OMNC-700 is stable for recycling and exhibits high efficiency in FA
9
10 dehydrogenation. Co@OMNC-700 is also a high-performance catalyst in the transfer
11
12 hydrogenation of various unsaturated hydrocarbons. On the contrary, without the protection of
13
14 OMNC, the exposed Co NPs in a control catalyst, Co/OMNC-700, leads to obvious Co leaching
15
16 and low efficiency for the transfer hydrogenation of quinoline with FA.
17
18
19
20
21
22

23 **KEYWORDS:** nitrogen-doped carbon, cobalt, acid-tolerant, water, green chemistry
24
25
26
27

28 **1. INTRODUCTION**

29
30 The replacement of fossil energy sources by biomass for chemicals and fuels production is a
31
32 promising approach for generating less greenhouse gases and decreasing the impact of human
33
34 activity on nature.¹ For example, catalytic hydrogenations adopt a privileged position in the
35
36 methodological toolbox for the chemical industry.^{2,3} Traditional hydrogenation process requires
37
38 excess (orders of magnitude more) high-pressure fossil-derived H₂ that is difficult and dangerous
39
40 to control, often leading to over hydrogenated products.² On the contrary, a liquid state hydrogen
41
42 source, formic acid (FA), has considerable hydrogen content (4.4 wt%), which could be used as a
43
44 safe and convenient hydrogen source.⁴ More importantly, FA can be easily obtained through
45
46 biomass oxidation or hydrolysis.^{5,6} The hydrogen readily releases upon catalytic decomposition
47
48 of FA, which could make it as a green hydrogen source for catalytic transfer hydrogenation
49
50 (CTH) over suitable catalysts.⁷
51
52
53
54
55
56
57
58
59
60

1
2
3 FA could act as a hydrogen source through a catalytic dehydrogenation reaction
4 (HCOOH→H₂+CO₂).⁸ However, an alternative dehydration pathway (HCOOH→H₂O+CO)
5 generates CO that could poison metal-based catalysts.⁹ To avoid the CO pathway, the
6 dehydrogenation of FA with homogeneous metal compounds has been widely reported.¹⁰
7
8 However, the difficulty of recycle, the use of various additives and/or organic solvents limit their
9 practical large-scale application.¹¹ These disadvantages associated with homogeneous catalysts
10 are dramatically mitigated by heterogeneous catalysts. Among heterogeneous catalysts, precious
11 metals are extensively studied for FA dehydrogenation, such as palladium,^{8,12-18} platinum,^{19,20}
12 ruthenium,⁹ aurum-based²¹⁻²³ and bimetallic^{7,24} systems. Moreover, most precious metal-
13 catalyzed FA dehydrogenation reactions need the assistance of excess alkali compounds (e.g.,
14 Na/K salts, amines),^{22,25-27} which further increase the cost of products separation and
15 purification. Limited studies have been carried out on non-precious metal catalysts. Apart from
16 the poor activity of non-precious metal catalysts,^{28,29} the high polarity and strong acidity of FA
17 usually lead to severe leaching and irreversible deactivation of the catalysts.³⁰ For all of these
18 reasons, it is highly desirable to design a heterogeneous catalyst that is cheap, efficient and
19 acid/CO-tolerant for a base-free CTH with FA.

20
21
22 Nitrogen-doped carbon (NC) has superior acid-base tolerance, improved basicity, and
23 enhanced p-donor capability from nitrogen dopants. NC-supported non-precious metal catalysts
24 have already exhibited promising performance in a variety of organic transformations.^{31,32} Direct
25 carbonization of metal-coordinated polymers or MOFs under an inert gas can prepare such
26 catalysts, in which metal NPs were confined in a carbonaceous matrix.³³⁻³⁸ Although the direct-
27 carbonization method is effortless, it typically does not endow much control over the position of
28 the active centers and often leads to severe aggregation, which deteriorates the performance and
29

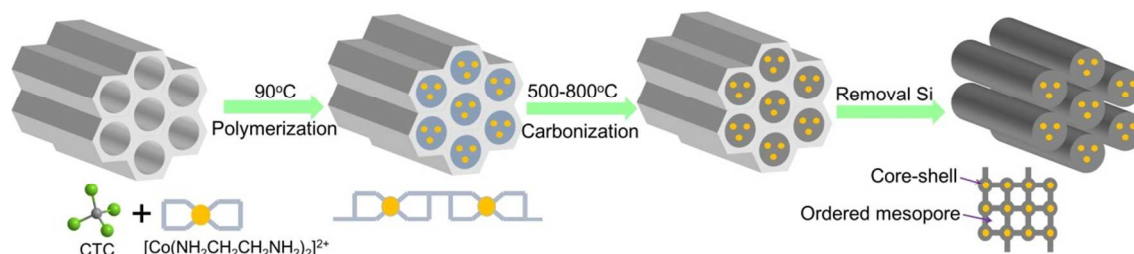
1
2
3 stability of catalysts.^{33,39} Additionally, direct coarse pyrolysis could destruct the pore structure of
4
5 the original supports that hinder the access for reactants to active centers.^{40,41}
6

7
8 Effective design of the precursors to endow the NC-based materials with multifunctional and
9
10 dispersed active sites that are easily reachable by substrates could significantly ameliorate the
11
12 previous problems and boost their catalytic performance.^{42,43} Herein, we synthesize ordered
13
14 mesoporous N-doped carbon (OMNC)-encapsulated Co (Co@OMNC) catalysts, in which Co is
15
16 encapsulated in OMNC by carbonizing the rationally designed Co-CN polymer@SBA-15
17
18 precursor. The resulted Co@OMNC catalyst has a high surface area ($543.2 \text{ m}^2 \text{ g}^{-1}$) and ordered
19
20 mesopores (4.6 nm) favoring the easy access of reactants. The as-obtained catalysts with
21
22 multiple active sites are highly efficient for coupling FA dehydrogenation with CTH of quinoline
23
24 under a base-free condition to produce 1,2,3,4-tetrahydroquinoline (THQ). Moreover, the
25
26 OMNC shell isolates the cobalt species from the acidic reaction media, and thus prevents Co
27
28 from poisoning or leaching. THQ is a key biologically active intermediate broadly used in the
29
30 production of many drugs and pesticides.⁴⁴⁻⁴⁶ Similar approaches (Scheme S1) for the synthesis
31
32 of THQ had been demonstrated using precious metal catalysts (Au, Rh, Pd), which requires large
33
34 amount of FA, high temperature ($>150 \text{ }^\circ\text{C}$), or assistance of excess bases (such as triethylamine,
35
36 HCO_2Na).^{11,22,47,48} The non-precious-metal-based Co@OMNC catalyst is highly efficient for the
37
38 CTH of quinoline, whose activity is comparable to the best precious-metal-based catalysts.
39
40
41
42
43
44
45

46 **2. RESULTS AND DISCUSSION**

47 **2.1. Structural characterizations**

48
49
50
51
52
53
54
55
56
57
58
59
60



Scheme 1 The synthesis process of Co@OMNC-x composites.

Co@OMNC catalysts were constructed by using SBA-15 as the template through a simple polymerization approach (**Scheme 1**). During this procedure, we used ethylenediamine (EDA) to capture Co^{2+} and generate $[\text{Co}(\text{EDA})_2]^{2+}$. Upon polymerization between EDA and carbon tetrachloride (CTC), Co-CN polymer filled into the mesopore of SBA-15. After carbonization and HF etching to simultaneously remove SBA-15 and unwrapped Co species, ordered mesoporous N-doped carbon-encapsulated Co catalysts were prepared.

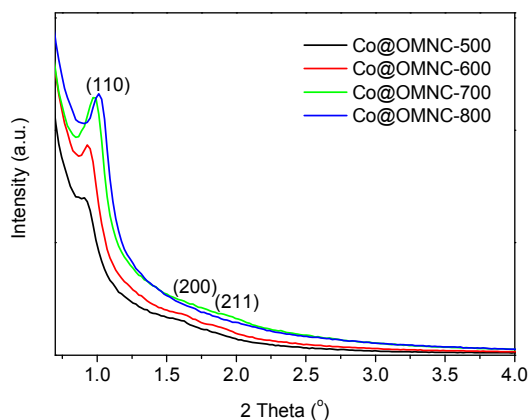


Figure 1. SAXRD patterns of Co@OMNCs.

The small angle X-ray diffraction (SAXRD) patterns of Co@OMNC-x shown in Figure 1 suggest the two-dimensional hexagonal $p6mm$ featured (110), (200), and (211) diffractions with 2θ below 2.5° .⁴⁹ The reflections gradually shift to higher 2θ values by increasing the pyrolysis

temperature (Table S1). As the carbonization temperature increases from 500 to 700 °C, the (110) diffraction becomes more intense, indicating that the increase of structural order at 700 °C. However, the (110) peak becomes less resolved at 800 °C, suggesting the slight destruction of the ordered mesostructure at high pyrolysis temperature.

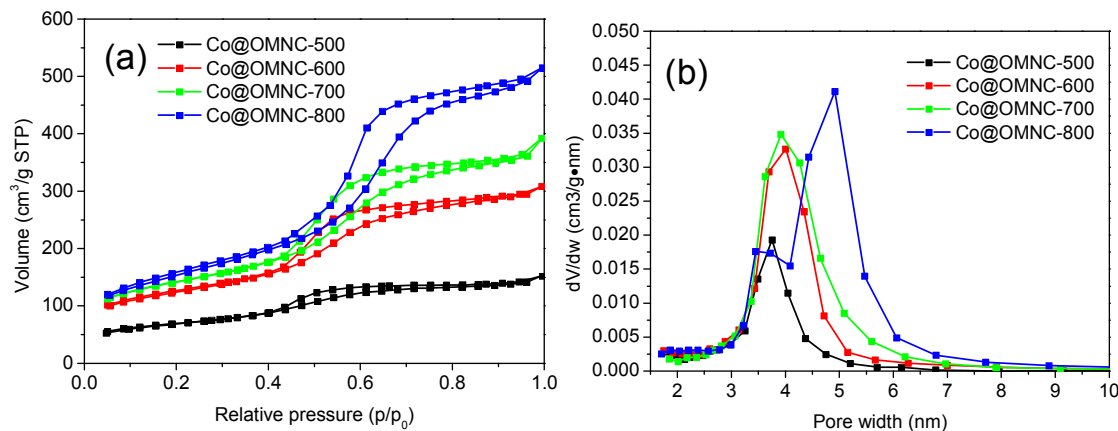


Figure 2. (a) N₂ sorption isotherms and (b) the size distributions of the mesoporous Co@OMNCs.

Table 1. Structural properties of the Co@OMNCs.

Samples	S_{total} (m ² /g)	Pore volume (cm ³ /g)	Average pore diameter (nm)
Co@OMNC-500	240	0.24	3.9
Co@OMNC-600	420	0.49	4.2
Co@OMNC-700	490	0.62	4.6
Co@OMNC-800	540	0.81	4.7

Figure 2a shows that all Co@OMNC-x samples display a type IV N₂ sorption isotherm, confirming the mesoporous nature of the catalysts.⁵⁰ As the pyrolysis temperature increases from 500 to 800 °C, the isotherms upraise obviously at the range of 0.5-0.9 p/p_0 , indicating the increased porosity of Co@OMNC-x. For instance, Co@OMNC-800 exhibits the highest surface area (540 m²/g) and pore volume (0.81 cm³/g) as shown in Table 1. Meanwhile, high pyrolysis temperature leads to broad pore size distribution (PSD) and hysteresis loop (Figure 2b). For

1
2
3 example, besides the main distribution at about 3.6 nm, Co@OMNC-800 also shows an
4 additional distribution within the range 4-7 nm. These results indicate that high temperature
5 could promote pore formation in Co@OMNC-x but partially destroy the long-range order of
6 their mesostructure,⁵¹ agreeing with the SAXRD results (Figure1).
7
8
9

10
11
12 The scanning electron microscopy (SEM) image of Co@OMNC-x (Figure S1a) shows that the
13 void spaces and the morphology of OMNC are analogous to the parent SBA-15. The high-
14 resolution SEM image (Figure S1b) further exhibits that mesopore channels are periodically
15 aligned over a large domain. The transmission electron microscopy (TEM) images in Figure 3
16 show that all Co@OMNC-x catalysts have uniformly distributed mesopores. We did not observe
17 any obvious Co NPs in Co@OMNC-500 (Figure S2). Increasing the pyrolysis temperature
18 a□ords the formation of large Co NPs with broad size distribution. The average particle sizes in
19 Co@OMNCs prepared at 600, 700, and 800 °C are 5.7, 14.1 and 18.4 nm, respectively. TEM
20 images of Co@OMNC-700 and Co@OMNC-600 show that, apart from the presence of
21 relatively large Co NPs up to ~15 nm, ultrasmall nanoclusters (~1 nm) are well dispersed in
22 mesopores in most areas (as shown in Figures 3b, d, and S3). HRTEM image shows that Co NPs
23 are embedded in mesoporous carbon skeleton. Figure 3e shows a representative Co NP with
24 0.215 nm interplanar spacing corresponding to the Co(111) plane, and the Co NP is embedded
25 by graphitic layers with a C(002) lattice plane (0.341 nm). As observed in the elemental mapping
26 of Co@OMNC-700 (Figure 3h), there is a good spatial overlap of C, N and Co elements,
27 demonstrating that N species and Co NPs distribute homogeneously over the mesoporous
28 carbon. The unique structure composed of ordered mesoporous N-doped carbon with
29 encapsulated Co NPs could favor the electron transferring, and restrain the leaching and
30 poisoning of Co NPs,⁴⁶ and thereby improve their catalytic stability and activity.
31
32
33
34
35
36
37
38
39
40
41
42
43
44
45
46
47
48
49
50
51
52
53
54
55
56
57
58
59
60

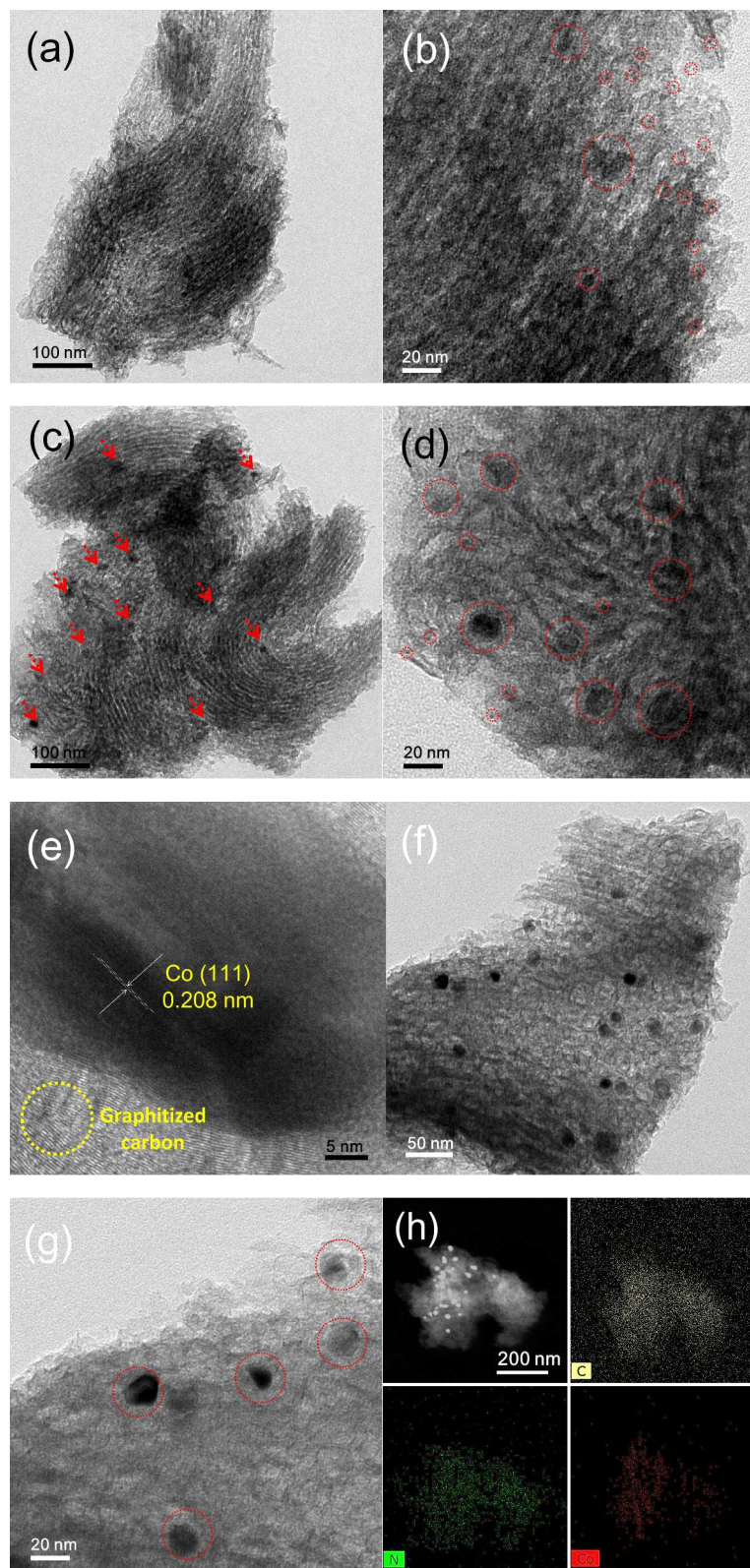


Figure 3. TEM images of Co@OMNC- (a,b) 600, (c-e) 700, (f,g) 800, and (h) elemental mapping of Co@OMNC-700.

We measured the wide-angle XRD patterns of Co@OMNCs (Figure S4), which show that the intensity of C(002) peak increases at high pyrolysis temperature. At 500 °C, no Co or CoO_x diffractions can be observed, while higher pyrolysis temperatures (600, 700, and 800 °C) lead to distinct diffraction peak from metallic Co. These results suggest that ionic Co is reduced *in situ* by carbon and/or nitrogen species during the high-temperature pyrolysis.⁵²

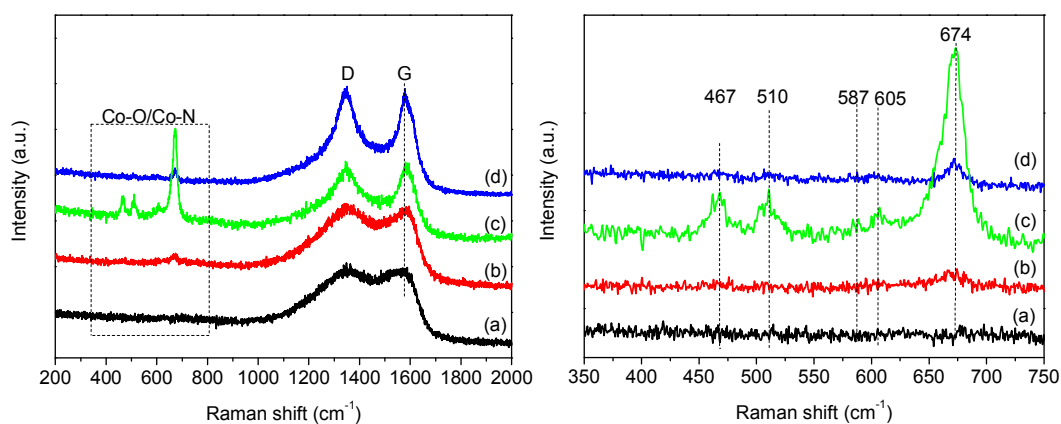


Figure 4. Raman spectra of Co@OMNC- (a) 500, (b) 600, (c) 700, and (d) 800.

The Raman spectra (Figure 4) clearly illustrate that the G peak sharpens and upshifts to higher wavenumber as the pyrolysis temperature increases, which indicates higher graphitization of carbon skeleton at higher pyrolysis temperature.^{33,53} At the same time, we also observed Co-N/Co-O vibration peaks at 400-700 cm⁻¹. Comparing with Co@OMNC-500 and Co@OMNC-600, Co@OMNC-700 shows stronger characteristic peaks, implying the enhanced N/O-Co interaction in Co@OMNC-700.⁵⁴ Further raising the temperature to 800 °C weakens these peaks (Figure 4d), indicating more Co⁰ is formed by the decomposition of Co-O/Co-N under high pyrolysis temperature, well agreed with the XRD results (Figure S4).

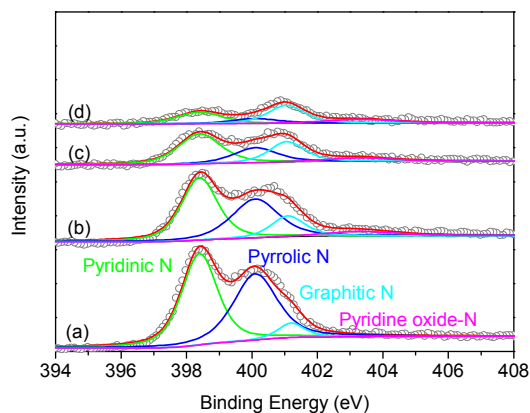


Figure 5. N1s spectra of Co@OMNC- (a) 500, (b) 600, (c) 700, and (d) 800.

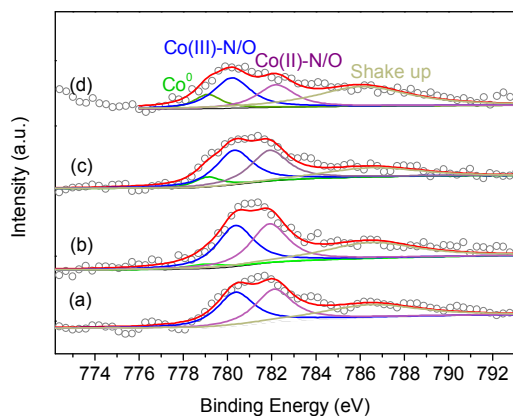


Figure 6. Co2p spectra of Co@OMNC- (a) 500, (b) 600, (c) 700, and (d) 800.

Table 2. Structural properties of Co@OMNC-x.

Catalysts	Relative atomic percentage of N (%)				Relative atomic percentage of Co (%)		
	Pyridinic N	Pyrrolic N	Graphitic N	Pyridine oxide-N	Co ⁰	Co(III)-N/O	Co(II)-N/O
Co@OMNC-500	50.0	44.1	5.9	0	0	50.7	49.3
Co@OMNC-600	44.4	35.6	13.8	6.2	4.2	52.6	43.2
Co@OMNC-700	44.5	22.8	25.1	7.58	7.9	50.8	41.3
Co@OMNC-800	31.2	14.1	39.6	15.1	16.8	47.7	35.5

The surface composition of Co@OMNC-x is detected by XPS. The C1s XPS peaks (Figure S5) of Co@OMNC-x become narrow and show an obvious shift to lower binding energy as elevating temperature from 500 to 800 °C, indicating the removing of nitrogen or oxygen species

from the catalysts.⁵⁵ The XPS data (Table S2, Figure S6) show that N contents of Co@OMNC-x decrease gradually with raising the pyrolysis temperature. We deconvoluted the XPS N1s peaks of Co@OMNC-x (Figure 5) into four types, pyridinic (398.5 eV), pyrrolic (400.1 eV), graphitic (401.1 eV), and pyridine oxide (403.3 eV).⁵⁶ The pyrrolic and pyridinic N are the dominate species (> 80 %) in Co@OMNC-500 and -600 (Table 2), but their percentages drop significantly to 67.3 % and 45.3 % in Co@OMNC-700 and -800, indicating the partial removal of non-stable pyridinic and pyrrolic N atoms under high-temperature pyrolysis.⁵²

We fitted the Co 2p_{3/2} XPS spectra of Co@OMNCs (Figure 6) with three Co species, Co⁰ (778.7 eV), Co(III)-N/O (780.6 eV), and Co(II)-N/O (782.6 eV).³⁹ The presence of Co-O/Co-N could be due to the coordination of cobalt ions with N/O in N-doped carbon that could be partially reserved during the carbonization process.⁵⁷ The percentage of Co(III)-N/O increases slightly from 50.7 to 52.6 % with increasing the pyrolysis temperature from 500 to 600 °C, but decreases to 47.7 % at 800 °C (Table 2). XPS could not detect any Co⁰ in Co@OMNC-500, while 4.2, 7.9 and 16.8 % Co⁰ is detected in Co@OMNC-600, Co@OMNC-700 and Co@OMNC-800, respectively. These results suggest that, as the pyrolysis temperature increases, Co-O and Co-N_x species are reduced *in situ* into Co⁰ by OMNC.⁵²

2.2 Transfer hydrogenation of quinoline with FA

Table 3. Performance of different catalysts in the hydrogenation of quinoline.^a

Entry	Catalysts	Hydrogen source	Solvent	T/ °C	Conversion / %	THQ selectivity / %
1	OMNC-700	FA	H ₂ O	140	-	-
2	Co@OMNC-700	none	H ₂ O	140	-	-
3	Co@OMNC-500	FA	H ₂ O	140	19.9	66.7
4	Co@OMNC-600	FA	H ₂ O	140	84.6	>99

5	Co@OMNC-700	FA	H ₂ O	140	98.8	>99
6	Co@OMNC-800	FA	H ₂ O	140	79.5	>99
7	Co@OMNC-700	FA	H ₂ O	130	51.7	>99
8	Co@OMNC-700	FA	H ₂ O	120	35.6	>99
9	Co@OMNC-700	FA	H ₂ O	110	26.8	>99
10	Co@OMNC-700	FA	Cyclohexane	140	44.5	>99
11	Co@OMNC-700	FA	THF	140	33.8	>99
12	Co@OMNC-700	FA	Ethanol	140	9.4	>99
13	Co@NC-700 ^b	FA	H ₂ O	140	25.9	>99
14	Co/AC	FA	H ₂ O	140	4.9	>99
15	Co/OMNC-700 ^c	FA	H ₂ O	140	36.7	>99
16	Co@OMNC-700	H ₂	H ₂ O	140	33.1	>99

^a Reaction conditions: quinoline (0.5 mmol), Co loading 10.6 mol%, FA (200 mg), H₂O (10 mL), N₂ 0.5 MPa, 140 °C, 4 h.

^b Prepared without SBA-15.

^c Prepared by impregnation method.

Table 3 shows the performance of different catalysts in quinoline CTH using FA or H₂ as the reducing agent at 140 °C (Table 3). No transformation of quinoline occurs when no metal or no FA is added (entries 1 and 2, Figure S7). With FA as the hydrogen source, catalysts with different carbonization temperature demonstrate a distinct difference in activity. For example, Co@OMNC-500 gives only 19.9 % quinoline conversion and 66.7 % THQ selectivity (entry 3). As the pyrolysis temperature increases, quinoline conversion increases obviously for Co@OMNC-700 with 98.8 % conversion along with 100 % THQ selectivity (entry 5). However, Co@OMNC-800 only gives 79.5 % quinoline conversion (entry 6). We also prepared another two control catalysts, disordered N-doped carbon supported Co (Co@NC-700) prepared without using a SBA-15 template and active carbon supported Co (Co/AC) prepared by impregnation

method. Both of the two catalysts showed much lower quinoline conversion (entries 13 and 14) than Co@OMNC-700 (entry 5) under the same condition, indicating the mesoporous structure in Co@OMNC-700 is beneficial for the substrate to access the active sites, thus improving their catalytic activity. As for reference, OMNC-700 is prepared firstly (entry 15), and then loaded by Co NPs to give Co/OMNC-700, the result shows only 36.7 % quinoline conversion (Figure S8), which is much lower than that of embedded Co@OMNC-700. Using molecular hydrogen (entry 16 and Figure S9), Co@OMNC-700 affords only 33.1 % quinoline conversion, indicating that the FA is more efficiently activated and dissociated than molecular H₂ to generate adsorbed hydrogen atoms for quinoline hydrogenation.⁵⁸

Temperature is an important parameter for this reaction (Table 3). For Co@OMNC-700, reducing reaction temperature from 140 to 110 °C leads to a substantial drop in quinoline conversion from 98.8 to 26.7 % (entries 7-9), while the THQ selectivity keeps almost constant. We also studied the effect of solvents, which also largely affect the reaction rate.⁵⁹ The survey shows (entries 5, 10-12) that water provides better conversion than ethanol, cyclohexane, and THF. Water is a green solvent that is eco-friendly and inexpensive.⁴⁷

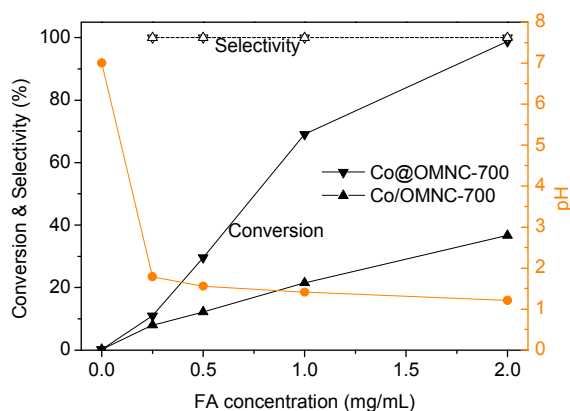
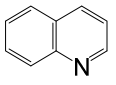
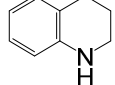
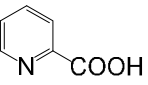
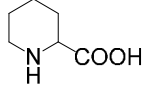
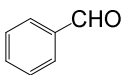
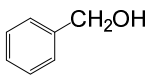
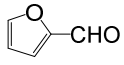
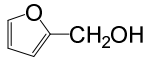
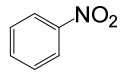
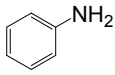
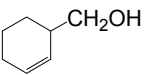
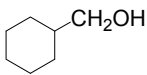
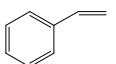
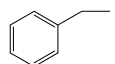


Figure 7. The transfer hydrogenation of quinoline and the solution pH affected by FA concentration. Reaction conditions: quinoline (0.5 mmol), Co loading 10.6 mol%, H₂O (10 mL), N₂ 0.5 MPa, 140 °C, 4h.

The FA concentration is another important factor in this reaction. Figure 7 shows the CTH of quinoline with different FA concentration over Co@OMNC-700 and Co/OMNC-700 catalysts. With the FA concentration increasing from 0 to 0.25 mg/mL, these two catalysts give similar reaction rates. However, further increase the FA concentration leads to a significant difference in conversion between Co@OMNC-700 and Co/OMNC-700, showing the feeble activity of Co/OMNC-700 under high FA concentration. Considering the strong acidity of FA, the pH of different FA solution is tested. We found that, as the FA concentration increases, pH value decreases obviously and reaches 1.21 when 2 mg/mL FA was used. It seems that unwrapped Co/OMNC-700 is more sensitive than Co@OMNC-700 under the strong acidic condition. We found that, after the reaction, the filtrate of Co/OMNC-700 turns to purple color (Figure S10). UV-vis spectrum (Figure S11) shows a significant light absorbance for Co/OMNC-700 in the range of 400-600 nm, implying Co species in Co/OMNC-700 partially dissolve in an acidic environment. On the contrary, no absorption peak appears for Co@OMNC-700, which indicate the OMNC shell prevents Co from contacting the acidic solution and thus avoids the possibility of etching or deactivation.⁶⁰ Additionally, the strong interaction between OMNC and inner Co leads to the superior performance of Co@OMNCs in CTH.⁵⁷ It is worth to point out that surface N-coordinated Co(II/III) sites could also involve in the catalysis,⁶¹ which requires more characterization.

Table 4. The CTH performance of Co@OMNC-700 for unsaturated hydrocarbons.^a

Entry	Substrate	Product	T/°C	t/h	Conversion/%	Selectivity/%
-------	-----------	---------	------	-----	--------------	---------------

1			140	4	98.8	>99
2			160	4	98.9	>99
3			160	6	95.4	>99
4			140	4	90.9	98.5
5			140	4	92.3	>99
6			140	4	99.2	>99
7			140	4	96.4	>99
8			140	6	100	>99

^a Reaction conditions: substrate (0.5 mmol), Co loading 10.6 mol%, FA (200 mg), H₂O (10 mL), N₂ 0.5 MPa.

The reaction scope in Table 4 demonstrates that Co@OMNC-700 is a versatile catalyst for the CTH of different unsaturated compounds in water. For N-heterocycle-like pyridine and 2-picolinic acid (entries 2 and 3), the catalyst affords good catalytic activity and the yields of piperidine are greater than 95%. In the case of benzaldehyde and furfural (entries 4 and 5), the reaction gives >90% conversion as well as >98% alcohol selectivity. Because of the great importance of aniline (AN), CTH of nitrobenzene (NB) is carried out (entry 6). It is found that 99.2% NB conversion as well as nearly 100% AN selectivity could be achieved within 4 h. Additionally, we also achieved high yield for the CTH of conjugated olefins (entries 7 and 8).

To study the activity difference for the CTH of quinoline, FA dehydrogenation over various catalysts is investigated (Figures S12 and S13). It is found that Co@OMNC-500, -600, -700 and

1
2
3 -800 afford 40.6, 72.5, 100 and 84% FA conversion, respectively. Comparatively, only 61.6 %
4
5 FA conversion can be observed over Co/OMNC-700. The FA dehydrogenation trend agrees with
6
7 the CTH of quinoline.
8
9

10 Considering the rich N species and ordered mesopore structure of Co@OMNC, the adsorption
11 capacity towards quinoline is measured by UV-vis (Figure S14). The amount of saturate
12 quinoline adsorption (Figure S15) over Co@OMNCx follows the order of Co@OMNC-500 < -
13 800 < -600 < -700, reaching maximum of 57.46 mg/g for Co@OMNC-700. The trend of
14 quinoline adsorption amount also agrees with the order of hydrogenation activity. We also used
15 CO₂-TPD to characterize the surface basicity of the Co@OMNC catalysts. The CO₂-TPD profiles
16 (Figure S16) show that there is one broad CO₂ desorption peak appearing at 300–500 °C for all
17 samples, which represents the desorption of chemical adsorbed CO₂ molecules over N species.⁵²
18 Comparatively, the CO₂ desorption peak becomes stronger for Co@OMNC-700. For Co@OMNC-
19 800, however, the CO₂ desorption peak weakens considerably, which could be attributed to the
20 decreased N content (especially for pyridinic N) resulting from the high preparation temperature.
21 Therefore, the good catalytic activity of Co@OMNC-700 could be related to the following two
22 reasons, 1) the favorable interaction between quinoline and the catalyst leads to the high
23 quinoline concentration on the surface of OMNC-700; and 2) the high density of basic sites on
24 the surface of OMNC-700 could enhance the adsorption and dehydrogenation of FA during the
25 CTH of quinoline.⁸
26
27
28
29
30
31
32
33
34
35
36
37
38
39
40
41
42
43
44
45
46
47
48
49
50
51
52
53
54
55
56
57
58
59
60

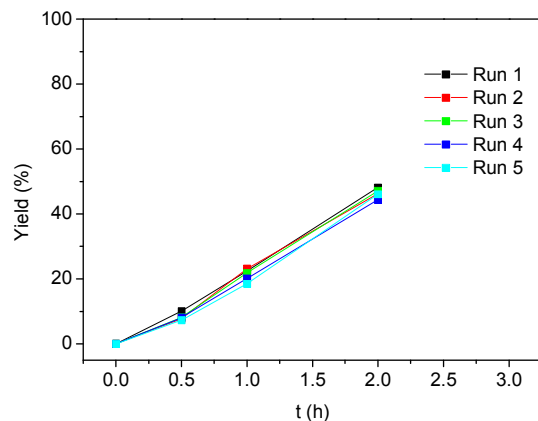


Figure 8. Durability test for the Co@OMNC-700 for transfer hydrogenation of quinoline with FA. Reaction conditions: quinoline (0.5 mmol), Co loading 10.6 mol%, FA (200 mg), H₂O (10 mL), N₂ 0.5 MPa, 140 °C.

The heterogeneous catalyst Co@OMNC-700 can be readily reused in the CTH of quinoline. There is no obvious loss in the conversion of quinoline over five runs with >90% conversion (Figure S17). To further confirm the stability of the catalyst, we also evaluated the reusability of Co@OMNC-700 by kinetics in CTH run to approximately 50 % conversion. The Co@OMNC-700 shows no sign of deactivation for five runs (Figures 8 and S18). The elemental analysis (Table S3) of the reused catalyst only shows less than 0.1 % Co leaching in the reaction solution, indicating that the OMNC can prevent the leaching of Co even in the acidic reaction solution at the elevated temperature. We characterized the used Co@OMNC-700 using XRD and XPS. Both the XRD pattern (Figure S19) and Co 2p XPS results (Figure S20 and Table S4) are similar to the fresh catalyst, which indicates the Co species in Co@OMNC-700 do not change significantly after five catalytic reaction runs. This result indicates that N-doped carbon layers could protect Co⁰ from etching by FA and strengthen the stability of Co NPs. Therefore, Co@OMNC-700 is indeed an acid-tolerant, cheap, and efficient catalyst in water media.

3. CONCLUSION

We demonstrated that Co NPs encapsulated in ordered mesoporous N-doped carbon (Co@OMNC) are efficient bifunctional heterogeneous catalysts for the transfer hydrogenation of quinoline to THQ using FA. Within all studied catalysts, Co@OMNC-700 shows the best activity and THQ selectivity using FA as the hydrogen source. A catalyst prepared by the simple impregnation of Co on OMNC-700 affords very poor performance due to severe leaching of Co active sites in acidic media. The unique catalytic property of Co@OMNC-700 for CTH of quinoline with FA is due to the well-designed structure composed of OMNC with encapsulated cobalt, in which the cobalt induces OMNC shell to be new active centers for both FA dehydrogenation and quinoline hydrogenation. With this structure, Co@OMNC-700 afforded superior acid-tolerance in the existence of FA and enhanced adsorption of substrates. The Co@OMNC-700 also shows high versatility for the CTH of various unsaturated hydrocarbons.

AUTHOR INFORMATION

Corresponding Author

*E-mail: refinie@163.com, whuang@iastate.edu

Notes

The authors declare no competing financial interest.

ASSOCIATED CONTENT

Supporting Information

The Supporting Information is available free of charge on the ACS Publications website at DOI:
10.1021/acscatal.

Experimental details, Tables S1 to S4, Figs. S1 to S20 (PDF)

ACKNOWLEDGMENTS

This work was supported by National Natural Science Foundation of China (21603066, 21606075), Natural Science Fund of Hubei Province (2015CFB232) and Natural Science Fund of the Education Department of Hubei Province (Q2015009). R. Nie thanks the China Scholarship Council and Hubei Chenguang Talented Youth Development Foundation for financial support.

REFERENCES

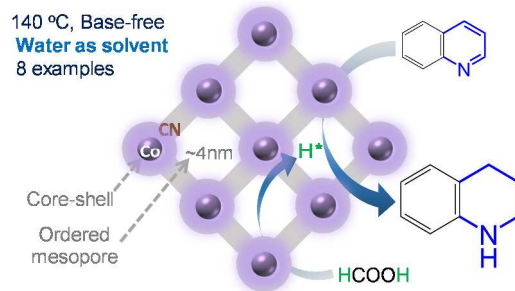
1. Gallezot, P. Conversion of Biomass to Selected Chemical Products. Conversion of Biomass to Selected Chemical Products. *Chem. Soc. Rev.* **2012**, *41*, 1538-1558.
2. Stanislaus, A.; Cooper, B. H. Aromatic Hydrogenation Catalysis: A Review. *Catal. Rev.* **1994**, *36*, 75-123.
3. Augustine, R. L. Organic Functional Group Hydrogenation. *Catal. Rev. Sci. Eng.* **1976**, *13*, 285-316.
4. Liu, X.; Li, S.; Liu, Y.; Cao, Y. Formic Acid: A Versatile Renewable Reagent for Green and Sustainable Chemical Synthesis. *Chin. J. Catal.* **2015**, *36*, 1461-1475.
5. Sun, Y.; Lin, L.; Pang, C.; Deng, H.; Peng, H.; Li, J.; He, B.; Liu, S. Hydrolysis of Cotton Fiber Cellulose in Formic Acid. *Energy Fuels* **2007**, *21*, 2386-2389.
6. Jin, F.; Yun, J.; Li, G.; Kishita, A.; Tohji, K.; Enomoto, H. Hydrothermal Conversion of Carbohydrate Biomass into Formic Acid at Mild Temperatures. *Green Chem.* **2008**, *10*, 612-615.
7. Singh, A. K.; Hwang, Y.-H.; Kim, D.-P. Heterogeneous PdAg Alloy Catalyst for Selective Methylation of Aromatic Amines with Formic Acid under an Additive-free and Solvothermal One-pot Condition. *NPG Asia Mater.* **2015**, *7*, e222.
8. Bi, Q.-Y.; Lin, J.-D.; Liu, Y.-M.; He, H.-Y.; Huang, F.-Q.; Cao, Y. Dehydrogenation of Formic Acid at Room Temperature: Boosting Palladium Nanoparticle Efficiency by Coupling with Pyridinic-Nitrogen-Doped Carbon. *Angew. Chem. Int. Ed.* **2016**, *55*, 11849-11853.

9. Ruppert, A. M.; Jędrzejczyk, M.; Sneka-Płatek, O.; Keller, N.; Dumon, A. S.; Michel, C.; Sautet, P.; Grams, J. Ru Catalysts for Levulinic Acid Hydrogenation with Formic Acid as a Hydrogen Source. *Green Chem.* **2016**, *18*, 2014-2028.
10. Gladiali, S.; Alberico, E. Asymmetric Transfer Hydrogenation: Chiral Ligands and Applications. *Chem. Soc. Rev.* **2006**, *35*, 226-236.
11. Cabrero-Antonino, J. R.; Adam, R.; Junge, K.; Jackstell, R.; Beller, M. Cobalt-catalysed Transfer Hydrogenation of Quinolines and Related Heterocycles Using Formic Acid under mild Conditions. *Catal. Sci. Technol.*, **2017**, *7*, 1981-1985.
12. Jin, M.-H.; Oh, D.; Park, J.-H.; Lee, C.-B.; Lee, S.-W.; Park, J.-S.; Lee, K.-Y.; Lee, D.-W. Mesoporous Silica Supported Pd-MnO_x Catalysts with Excellent Catalytic Activity in Room-Temperature Formic Acid Decomposition. *Sci. Rep.* **2016**, *6*, 33502.
13. Jaya T.; Shun N.; Kohki E. Base-free Chemoselective Transfer Hydrogenation of Nitroarenes to Anilines with Formic Acid as Hydrogen Source by a Reusable Heterogeneous Pd/ZrP Catalyst. *RSC Adv.*, **2014**, *4*, 38241-38249
14. Zhang, D.; Ye, F.; Xue, T.; Guan, Y.; Wang, Y. M. Transfer Hydrogenation of Phenol on Supported Pd Catalysts Using Formic Acid as an Alternative Hydrogen Source. *Catal. Today* **2014**, *234*, 133-138.
15. Gong, L.-H.; Cai, Y.-Y.; Li, X.-H.; Zhang, Y.-N.; Su, J.; Chen, J.-S. Room-temperature Transfer Hydrogenation and Fast Separation of Unsaturated Compounds over Heterogeneous Catalysts in an Aqueous Solution of Formic Acid. *Green Chem.* **2014**, *16*, 3746-3751.
16. Yoo, J. S.; Zhao, Z.-J.; Nørskov, J. K.; Studt, F. Effect of Boron Modifications of Palladium Catalysts for the Production of Hydrogen from Formic Acid. *ACS Catal.* **2015**, *5*, 6579-6586.
17. Bulushev, D. A.; Zacharska, M.; Shlyakhova, E. V.; Chuvilin, A. L.; Guo, Y.; Beloshapkin, S.; Okotrub, A. V.; Bulusheva, L. G. Single Isolated Pd²⁺ Cations Supported on N-Doped Carbon as Active Sites for Hydrogen Production from Formic Acid Decomposition. *ACS Catal.* **2016**, *6*, 681-691.
18. Wang, L.; Zhang, B.; Meng, X.; Su, D. S.; Xiao, F.-S. Hydrogenation of Biofuels with Formic Acid over a Palladium-Based Ternary Catalyst with Two Types of Active Sites. *ChemSusChem* **2014**, *7*, 1537-1541.
19. Bulushev, D. A.; Zacharska, M.; Lisitsyn, A. S.; Podyacheva, O. Y.; Hage, F. S.; Ramasse, Q. M.; Bangert, U.; Bulusheva, L. G. Single Atoms of Pt-Group Metals Stabilized by N-Doped Carbon Nanofibers for Efficient Hydrogen Production from Formic Acid. *ACS Catal.* **2016**, *6*, 3442-3451.
20. Jia, L.; Bulushev, D. A.; Podyacheva, O. Y.; Boronin, A. I.; Kibis, L. S.; Gerasimov, E. Y.; Beloshapkin, S.; Seryak, I. A.; Ismagilov, Z. R.; Ross, J. R. H. Pt Nanoclusters Stabilized by N-doped Carbon Nanofibers for Hydrogen Production from Formic Acid. *J. Catal.* **2013**, *307*, 94-102.
21. Du, X.-L.; He, L.; Zhao, S.; Liu, Y.-M.; Cao, Y.; He, H.-Y.; Fan, K.-N. Hydrogen-Independent Reductive Transformation of Carbohydrate Biomass into γ -Valerolactone and Pyrrolidone Derivatives with Supported Gold Catalysts. *Angew. Chem. Int. Ed.* **2011**, *50*, 7815-7819.
22. Tao, L.; Zhang, Q.; Li, S.-S.; Liu, X.; Liu, Y.-M.; Cao, Y. Heterogeneous Gold-Catalyzed Selective Reductive Transformation of Quinolines with Formic Acid. *Adv. Syn. Catal.* **2015**, *357*, 753-760.

23. Son, P. A.; Nishimura, S.; Ebitani, K. Production of γ -Valerolactone from Biomass-derived Compounds using Formic Acid as a Hydrogen Source over Supported Metal Catalysts in Water Solvent. *RSC Adv.* **2014**, *4*, 10525-10530.
24. Gao, S.; Liu, W.; Feng, C.; Shang, N.; Wang, C. Exceptional Size-dependent Catalytic Activity Enhancement in the Room-temperature Hydrogen Generation from Formic Acid over Bimetallic Nanoparticles Supported by Porous Carbon. *Catal. Sci. Technol.*, **2016**, *6*, 869-874.
25. Vilches-Herrera, M.; Werkmeister, S.; Junge, K.; Börner, A.; Beller, M. Selective Catalytic Transfer Hydrogenation of Nitriles to Primary Amines Using Pd/C. *Catal. Sci. Technol.*, **2014**, *4*, 629-632.
26. Wei, Y.; Wang, C.; Jiang, X.; Xue, D.; Liu, Z.-T.; Xiao, J. Catalyst-free Transformation of Levulinic Acid into Pyrrolidinones with Formic Acid. *Green Chem.* **2014**, *16*, 1093-1096.
27. Talwar, D.; Li, H. Y.; Durham, E.; Xiao, J. A Simple Iridacycle Catalyst for Efficient Transfer Hydrogenation of N-Heterocycles in Water. *Chem. A Eur. J.* **2015**, *21*, 5370-5379.
28. Upare, P. P.; Jeong, M.-G.; Hwang, Y. K.; Kim, D. H.; Kim, Y. D.; Hwang, D. W.; Lee, U. H.; Chang, J.-S. Nickel-promoted Copper-silica Nanocomposite Catalysts for Hydrogenation of Levulinic Acid to Lactones Using Formic Acid as a Hydrogen Feeder. *Appl. Catal., A* **2015**, *491*, 127-135.
29. Yuan, J.; Li, S.; Yu, L.; Liu, Y.; Cao, Y. Efficient Catalytic Hydrogenolysis of Glycerol Using Formic Acid as Hydrogen Source. *Chin. J. Catal.* **2013**, *34*, 2066-2074.
30. Yang, Y.; Gao, G.; Zhang, X.; Li, F. Facile Fabrication of Composition-Tuned Ru-Ni Bimetallics in Ordered Mesoporous Carbon for Levulinic Acid Hydrogenation. *ACS Catal.* **2014**, *4*, 1419-1425.
31. Li, X.-H.; Antonietti, M. Metal Nanoparticles at Mesoporous N-doped Carbons and Carbon Nitrides: Functional Mott-Schottky Heterojunctions for Catalysis. *Chem. Soc. Rev.* **2013**, *42*, 6593-6604.
32. Wang, X.; Sun, G.; Routh, P.; Kim, D.-H.; Huang, W.; Chen, P. Heteroatom-doped Graphene Materials: Syntheses, Properties and Applications. *Chem. Soc. Rev.* **2014**, *43*, 7067-7098.
33. Shen, K.; Chen, X.; Chen, J.; Li, Y. Development of MOF-Derived Carbon-Based Nanomaterials for Efficient Catalysis. *ACS Catal.* **2016**, *6*, 5887-5903.
34. Shi, J.; Wang, Y.; Du, W.; Hou, Z. Synthesis of Graphene Encapsulated Fe₃C in Carbon Nanotubes from Biomass and Its Catalysis Application. *Carbon* **2016**, *99*, 330-337.
35. Yang, H.; Nie, R.; Xia, W.; Yu, X.; Jin, D.; Lu, X.; Zhou, D.; Xia, Q. Co Embedded within Biomass-Derived Mesoporous N-doped Carbon as an Acid-resistant and Chemoselective Catalyst for Transfer Hydrodeoxygenation of Biomass with Formic Acid. *Green Chem.* **2017**, *19*, 5714-5722.
36. Lu, G.; Li, S.; Guo, Z.; Farha, O. K.; Hauser, B. G.; Qi, X.; Wang, Y.; Wang, X.; Han, S.; Liu, X.; DuChene, J. S.; Zhang, H.; Zhang, Q.; Chen, X.; Ma, J.; Loo, S. C. J.; Wei, W. D.; Yang, Y.; Hupp, J. T.; Huo, F. Imparting Functionality to a Metal-Organic Framework Material by Controlled Nanoparticle Encapsulation. *Nat. Chem.* **2012**, *4*, 310-316.
37. Wu, Z.-Y.; Hu, B.-C.; Wu, P.; Liang, H.-W.; Yu, Z.-L.; Lin, Y.; Zheng, Y.-R.; Li, Z.; Yu, S.-H. Mo₂C Nanoparticles Embedded within Bacterial Cellulose-Derived 3D N-Doped Carbon Nanofiber Networks for Efficient Hydrogen Evolution. *NPG Asia Mater.* **2016**, *8*, e288.

- 1
2
3
4
5
6
7
8
9
10
11
12
13
14
15
16
17
18
19
20
21
22
23
24
25
26
27
28
29
30
31
32
33
34
35
36
37
38
39
40
41
42
43
44
45
46
47
48
49
50
51
52
53
54
55
56
57
58
59
60
38. Wei, J.; Liang, Y.; Hu, Y.; Kong, B.; Zhang, J.; Gu, Q.; Tong, Y.; Wang, X.; Jiang, S. P.; Wang, H. Hydrothermal Synthesis of Metal–Polyphenol Coordination Crystals and Their Derived Metal/N - doped Carbon Composites for Oxygen Electrocatalysis. *Angew. Chem. Int. Ed.* **2016**, *55*, 12470-12474.
 39. Bai, C.; Li, A.; Yao, X.; Liu, H.; Li, Y. Efficient and Selective Aerobic Oxidation of Alcohols Catalysed by MOF-derived Co Catalysts. *Green Chem.* **2016**, *18*, 1061-1069.
 40. Liang, X.; Quan, B.; Ji, G.; Liu, W.; Cheng, Y.; Zhang, B.; Du, Y. Novel Nanoporous Carbon Derived from Metal–Organic Frameworks with Tunable Electromagnetic Wave Absorption Capabilities. *Inorg. Chem. Front.* **2016**, *3*, 1516-1526.
 41. Jagadeesh, R. V.; Murugesan, K.; Alshammari, A. S.; Neumann, H.; Pohl, M.-M.; Radnik, J.; Beller, M. MOF-derived Cobalt Nanoparticles Catalyze a General Synthesis of Amines. *Science* **2017**, *358*, 326-332.
 42. Liu, J.; Wickramaratne, N. P.; Qiao, S. Z.; Jaroniec, M. Molecular-Based Design and Emerging Applications of Nanoporous Carbon Spheres. *Nat. Mater.* **2015**, *14*, 763-774.
 43. Wang, T.; Dong, Z.; Cai, W.; Wang, Y.; Fu, T.; Zhao, B.; Peng, L.; Ding, W.; Chen, Y. An Efficient Hydrogenation Catalyst in Sulfuric Acid for Nitrobenzene to p-Aminophenol: N-doped Carbon with Encapsulated Molybdenum Carbide. *Chem. Commun.* **2016**, *52* (70), 10672-10675.
 44. Graves, P. R.; Kwiek, J. J.; Fadden, P.; Ray, R.; Hardeman, K.; Coley, A. M.; Foley, M.; Haystead, T. A. Discovery of Novel Targets of Quinoline Drugs in the Human Purine Binding Proteome. *Mol. Pharm.* **2002**, *62*, 1364-1372.
 45. Fournet, A.; Barrios, A. A.; Munoz, V.; Hocquemiller, R.; Cavé, A.; Bruneton, J. 2-substituted Quinoline Alkaloids as Potential Antileishmanial Drugs. *Antimicrob. Agents Ch.* **1993**, *37*, 859-863.
 46. Wei, Z.; Chen, Y.; Wang, J.; Su, D.; Tang, M.; Mao, S.; Wang, Y. Cobalt Encapsulated in N-Doped Graphene Layers: An Efficient and Stable Catalyst for Hydrogenation of Quinoline Compounds. *ACS Catal.* **2016**, *6*, 5816-5822.
 47. Vilhanová, B.; van Bokhoven, J. A.; Ranocchiari, M. Gold Particles Supported on Amino-Functionalized Silica Catalyze Transfer Hydrogenation of N-Heterocyclic Compounds. *Adv. Syn. Catal.* **2017**, *359*, 677-686.
 48. Dell'Anna, M. M.; Capodiferro, V. F.; Mali, M.; Manno, D.; Cotugno, P.; Monopoli, A.; Mastroilli, P. Highly Selective Hydrogenation of Quinolines Promoted by Recyclable Polymer Supported Palladium Nanoparticles under Mild Conditions in Aqueous Medium. *Appl. Catal., A* **2014**, *481*, 89-95.
 49. Vinu, A. Two-Dimensional Hexagonally-Ordered Mesoporous Carbon Nitrides with Tunable Pore Diameter, Surface Area and Nitrogen Content. *Adv. Funct. Mater.* **2008**, *18*, 816-827.
 50. Wang, G.-H.; Cao, Z.; Gu, D.; Pfänder, N.; Swertz, A.-C.; Spliethoff, B.; Bongard, H.-J.; Weidenthaler, C.; Schmidt, W.; Rinaldi, R.; Schüth, F. Nitrogen-Doped Ordered Mesoporous Carbon Supported Bimetallic PtCo Nanoparticles for Upgrading of Biophenolics. *Angew. Chem. Int. Ed.* **2016**, *55*, 8850-8855.
 51. Jin, X.; Balasubramanian, V. V.; Selvan, S. T.; Sawant, D. P.; Chari, M. A.; Lu, G. Q.; Vinu, A. Highly Ordered Mesoporous Carbon Nitride Nanoparticles with High Nitrogen Content: A Metal-Free Basic Catalyst. *Angew. Chem. Int. Ed.* **2009**, *48*, 7884-7887.

- 1
2
3 52. Long, J.; Shen, K.; Li, Y. Bifunctional N-Doped Co@C Catalysts for Base-Free Transfer
4 Hydrogenations of Nitriles: Controllable Selectivity to Primary Amines vs Imines. *ACS*
5 *Catal.* **2017**, *7*, 275-284.
6
7 53. Nie, R.; Wang, J.; Wang, L.; Qin, Y.; Chen, P.; Hou, Z. Platinum Supported on Reduced
8 Graphene Oxide as a Catalyst for Hydrogenation of Nitroarenes. *Carbon* **2012**, *50*, 586-596.
9 54. Wang, L.; Zhang, J.; Yi, X.; Zheng, A.; Deng, F.; Chen, C.; Ji, Y.; Liu, F.; Meng, X.; Xiao,
10 F.-S. Mesoporous ZSM-5 Zeolite-Supported Ru Nanoparticles as Highly Efficient Catalysts
11 for Upgrading Phenolic Biomolecules. *ACS Catal.* **2015**, *5*, 2727-2734.
12 55. Nie, R.; Jiang, H.; Lu, X.; Zhou, D.; Xia, Q. Highly Active Electron-deficient Pd Clusters on
13 N-doped Active Carbon for Aromatic Ring Hydrogenation. *Catal. Sci. Technol.* **2016**, *6*,
14 1913-1920.
15 56. Jiang, H.; Yu, X.; Nie, R.; Lu, X.; Zhou, D.; Xia, Q. Selective Hydrogenation of Aromatic
16 Carboxylic Acids over Basic N-doped Mesoporous Carbon Supported Palladium Catalysts.
17 *Appl. Catal., A* **2016**, *520*, 73-81.
18 57. Chen, F.; Kreyenschulte, C.; Radnik, J.; Lund, H.; Surkus, A.-E.; Junge, K.; Beller, M.
19 Selective Semihydrogenation of Alkynes with N-Graphitic-Modified Cobalt Nanoparticles
20 Supported on Silica. *ACS Catal.* **2017**, *7*, 1526-1532.
21 58. Zhou, P.; Jiang, L.; Wang, F.; Deng, K.; Lv, K.; Zhang, Z. High Performance of a Cobalt-
22 Nitrogen Complex for the Reduction and Reductive Coupling of Nitro Compounds into
23 Amines and Their Derivatives. *Sci. Adv.* **2017**, *3*, e1601945.
24 59. Gong, Y.; Zhang, P.; Xu, X.; Li, Y.; Li, H.; Wang, Y. A Novel Catalyst Pd@ompg-C₃N₄ for
25 Highly Chemoselective Hydrogenation of Quinoline under Mild Conditions. *J. Catal.* **2013**,
26 *297*, 272-280.
27 60. Fu, T.; Wang, M.; Cai, W.; Cui, Y.; Gao, F.; Peng, L.; Chen, W.; Ding, W. Acid-Resistant
28 Catalysis without Use of Noble Metals: Carbon Nitride with Underlying Nickel. *ACS Catal.*
29 **2014**, *4*, 2536-2543.
30 61. Liu, W.; Zhang, L.; Yan, W.; Liu, X.; Yang, X.; Miao, S.; Wang, W.; Wang, A.; Zhang, T.
31 Single-Atom Dispersed Co-N-C Catalyst: Structure Identification and Performance for
32 Hydrogenative Coupling of Nitroarenes. *Chem. Sci.* **2016**, *7* (9), 5758-5764.
33
34
35
36
37
38
39
40
41
42
43
44
45
46
47
48
49
50
51
52
53
54
55
56
57
58
59
60

Graphic abstract

Ordered mesoporous N-doped carbon encapsulated Co is an acid-resistant catalyst for coupling biomass-derived FA dehydrogenation and quinoline hydrogenation in water solution under a base-free condition.